# Metal-insulator phase transitions of $SmNiO_3$ and $PrNiO_3$: Electrons in a polaronic medium

María Andrea Mroginski*
*Departamento de Física, Universidad Nacional del Nordeste, Avenida Libertad 5600, (3400) Corrientes, Argentina*

Néstor E. Massa†
*Laboratorio Nacional de Investigación y Servicios en Espectroscopía Optica, Centro CEQUINOR–Departamento de Química and Departamento de Física, Universidad Nacional de La Plata, C.C. 962, (1900) La Plata, Argentina*

Horacio Salva
*Comisión Nacional de Energía Atómica, Centro Atómico Bariloche and Instituto Balseiro, (8400) Bariloche, Rio Negro, Argentina*

José Antonio Alonso and María Jesús Martínez-Lope
*Instituto de Ciencias de Materiales de Madrid, Consejo Superior de Investigaciones Científicas, Cantoblanco, E-28049 Madrid, Spain*
(Received 22 January 1999)

Temperature dependence of reflectivity and transmission infrared spectra and photoinduced activity of $RNiO_3$ ($R$=Sm, Pr) were studied in order to elucidate the mechanism responsible for the metal-insulator transition at $T_{MI}\approx 135$ K and $\approx 403$ K, respectively. The reflectivity analysis and the agreement found between the small polaron theory and experimental conductivity allowed us to point out the electron-phonon interaction strength and therefore confirm the determinant participation of phonons in the transport properties of $RNiO_3$ ($R$=Pr, Sm). According to this, the metal-insulator transition at $T_{MI}$ is directly related to self-trapped electrons in a polaronic medium. [S0163-1829(99)02628-4]

## INTRODUCTION

Rare-earth ($R$) nickelates, belonging to the $ABO_3$ perovskite family, have been intensively studied in the past few years especially because the thermally driven metal-to-insulator (MI) phase transition they undergo as a function of the size of the rare-earth ion. $LaNiO_3$ is metallic in all the temperature range; $RNiO_3$ ($R$: rare earth) for $R^{3+}$ cations smaller than $La^{3+}$ show rather sharp metal-insulator phase transition at $T_{MI}$ followed by antiferromagnetic ordering and a small discontinuous decrease in the unit cell.[1]

Interest in the study of these compounds is very recent. First synthesized by Demazeau,[2] their physical and structural properties have not been studied until 1989. For the moment, only structural, magnetic, and electric properties of some of the members of the $RNiO_3$ family ($R$=Nd, Pr, Sm, and Eu) have been determined, and the possible mechanism responsible for the MI phase transition has been outlined.[1]

In order to understand the behavior of carriers when those structural, electronic, and magnetic changes take place at or near the critical temperature $T_{MI}$, we have analyzed the temperature dependence of the reflectivity, transmission and the photoinduced activity of $PrNiO_3$ and $SmNiO_3$ in the infrared spectral range. Interestingly, while $PrNiO_3$ undergoes the MI transition and the magnetic ordering simultaneously at about $T_{MI}=T_N\approx 135$ K; $SmNiO_3$ experiments the MI transition at $T_{MI}\approx 403$ K with the antiferromagnetic ordering appearing at only $T_N\approx 225$ K (Ref. 3). Although this magnetic transition is much weaker than in $PrNiO_3$ or $NdNiO_3$ the same propagation vector as in $NdNiO_3$ suggests similar behavior.[4]

Polycrystalline $PrNiO_3$ and $SmNiO_3$ pellets were prepared by a liquid-mixture technique. A stoichiometric mixture of metal nitrates was solved in citric acid and the citrate solution was then slowly decomposed at temperatures up to 600 °C. This black precursor was heated at 1000 °C under a 200 bars in an oxygen atmosphere for 12 h and cooled at room temperature, giving a polycrystalline powder that was pressed into 7 mm diameter pellets and sintered again at 1000 °C for 12 h under 200 bars in an $O_2$ atmosphere. These samples were characterized by x-ray and neutron powder diffraction, thermogravimetric analysis, differential scanning calorimetry, and resistivity measurements.[5]

We also characterized our samples between 4 and 300 K by four-point resistivity measurements. Their magnetic susceptibilities were measured with a Quantum Design (SQUID) magnetometer at 1000 G. These results are shown in Fig. 1 (full circles indicate the temperatures at which the reflectivities were measured). The resistivity plot shows a sharp MI transition for $PrNiO_3$, at $T_{MI}=135$ K, characterized

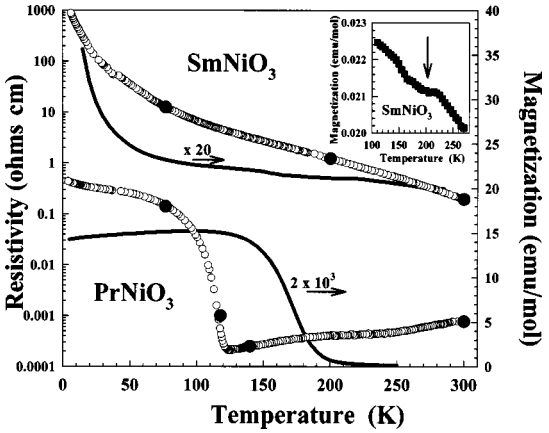


FIG. 1. Resistivity and magnetic susceptibility of $SmNiO_3$ and $PrNiO_3$. The inset shows the antiferromagnetic transition of $SmNiO_3$ at about 225 K. *Full circles* on the resistivity curves indicate the temperature at which the reflectivities were measured.

 

by an abrupt change of more than three orders of magnitude. Since for $SmNiO_3$ the equivalent MI transition takes place above room temperature, outside the resistivity measuring range, only the insulator regime is visible in the plot.

Near, medium, and far infrared reflectivity and transmission (Tr) spectra between 30–10 000 $cm^{-1}$ were measured at different temperatures in a FT-IR Bruker 113 v interferometer with 4 $cm^{-1}$ (FIR and MIR) and 6 $cm^{-1}$ (NIR) resolution. Semitransparent CsI and polyethylene 1-cm-diam pellets, embedded randomly with microcrystals, were made in order to determine the transmission spectra. Our samples were mounted on a cold finger of an OXFORD DN 1754 cryostat and for reflectivity measurements, a gold mirror was used as a 100% reference. The temperature stability was 0.1 K.

We estimated phonon frequencies and optical conductivities using a standard multioscillator dielectric simulation fit on our reflectivity spectra.[6] Pursuing further characterization of the electron-phonon interaction and exploring possible polaron formation, we fitted the experimental optical conductivity with a theoretical expression proposed by Reik and Heese small polaron theory.[7]

Irradiation of samples, while coadding 2000 spectra with 4 $cm^{-1}$ resolution, was achieved by illumination through an optical fiber bundle with the 4880 Å line of a cw $Ar^+$ laser. The laser power, measured at the output of the optical fiber bundle, was about 60 $mW/cm^2$.

## SPECTRAL ANALYSIS

We analyzed the reflectivity spectra simulating infrared-active features with damped Lorentzian oscillators in a classical formulation of the dielectric function. In addition, when the measured spectra required, one plasma contribution (Drude term) was added to the dielectric simulation.[6] The complete expression of the dielectric function together with the Drude term is given by

$$\varepsilon(\omega)=\varepsilon_\infty\prod_j\left[\frac{\omega_{j\mathrm{LO}}^2-\omega^2+i\gamma_{j\mathrm{LO}}\omega}{\omega_{j\mathrm{TO}}^2-\omega^2+i\gamma_{j\mathrm{TO}}\omega}\right]-\varepsilon_\infty\frac{[\omega_p^2+i(\gamma_p-\gamma_0)\omega]}{[\omega(\omega-i\gamma_0)]},\tag{1}$$

where $\varepsilon_\infty$ is the high-frequency dielectric function; $\omega_{j\mathrm{LO}}$ and $\omega_{j\mathrm{TO}}$ are the longitudinal and transverse $j$th optical frequencies with damping constants $\gamma_{j\mathrm{LO}}$ and $\gamma_{j\mathrm{TO}}$ respectively. The second term represents the Drude contribution where $\omega_p$ is the plasma frequency, $\gamma_p$ its damping, and $\gamma_o$ is understood as a phenomenological damping introduced by the lattice drag. We also calculated the $j$th oscillator strength $S_j$ as

$$S_j=\omega_{j\mathrm{TO}}^{-2}\frac{\Pi_k(\omega_{k\mathrm{LO}}^2-\omega_{j\mathrm{TO}}^2)}{\Pi_{k\neq j}(\omega_{k\mathrm{TO}}^2-\omega_{j\mathrm{TO}}^2)}.\tag{2}$$

With

$$\omega_p^2=4\pi e^2N/m^*,\tag{3}$$

we can estimate an effective carrier concentration $N^*=Nm_0/m^*$ ($m_0$ and $m^*$ are the free- and effective electron mass; $N$ and $N^*$ are the number and the effective number of carriers, respectively).

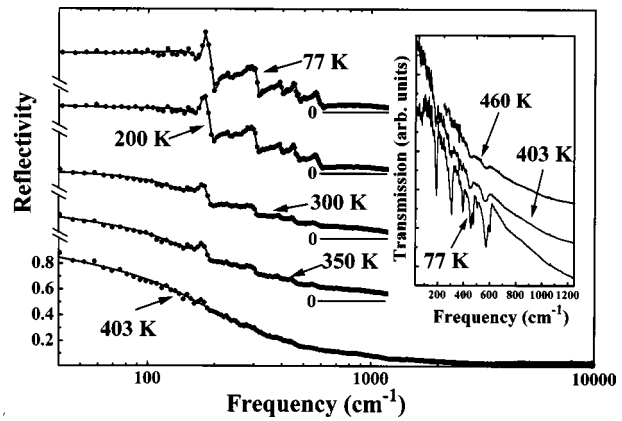


FIG. 2. Infrared reflectivity $SmNiO_3$. Dots, experimental measurements; full line, calculated reflectivity obtained by the dielectric simulation. The inset shows transmission spectra of $SmNiO_3$ at 77, 403, and 460 K. The highest-temperature far-infrared transmission measurement was limited up to about 400 K because pellets used in that spectral region are made of polyethylene.

To study the optical conductivity, $\sigma_1=(\omega/4\pi)\varepsilon_2$ ($\varepsilon_2$ is the imaginary part of the dielectric function) we used theoretical expressions for small polarons due to nondiagonal phonon transitions as calculated by Reik and Heese.[7] In this model optical properties are due to carriers in one small band and interband transitions are excluded. Starting with a Holstein's Hamiltonian[8] the frequency dependent conductivity is calculated using Kubo's formula.[9] Thus, the real part of the optical conductivity for finite temperature, $\sigma_1(\omega,\beta)$ is given by

$$\sigma_1(\omega,\beta)=\sigma_{\mathrm{dc}}\frac{\sinh\left(\frac{1}{2}\hbar\omega\beta\right)\exp[-\omega^2\tau^2r(\omega)]}{\frac{1}{2}\hbar\omega\beta[1+(\omega\tau\Delta)^2]^{1/4}},\tag{4}$$

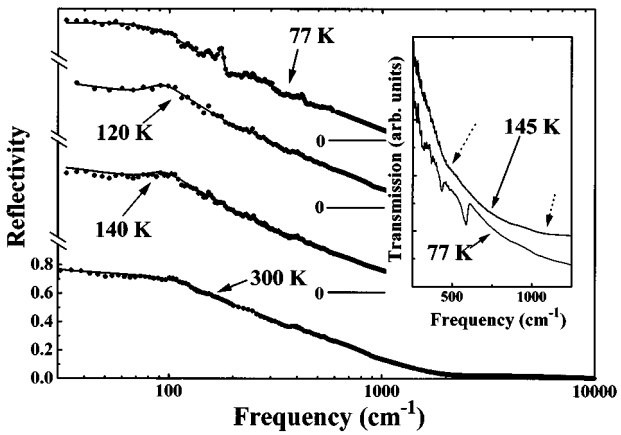


FIG. 3. Infrared reflectivity of $PrNiO_3$. Dots, experimental measurements; full line, calculated reflectivity obtained by the dielectric function simulation. The inset shows transmission spectra of $PrNiO_3$ above and below the $T_{\mathrm{MI}}$ phase transition. Dotted arrows point to two weak changes in the transmission spectra of the metallic phase associated with the phonon density of states and its overtone.

TABLE I. Fitting parameters used in the dielectric function simulation for $SmNiO_3$.

| Temperature (K) | $\varepsilon_\infty$ | $\omega_{TO}$ ($cm^{-1}$) | $\omega_{LOf}$ ($cm^{-1}$) $\omega_p$ ($cm^{-1}$) | $\gamma_{TO}$ ($cm^{-1}$) $\gamma_0$ ($cm^{-1}$) | $\gamma_{LO}$ ($cm^{-1}$) $\gamma_p$ ($cm^{-1}$) | $S$ ($cm^{-2}$) |
|---|---|---|---|---|---|---|
| | | 161.9 | 174.8 | 100.5 | 18.9 | 9.29 |
| | | 176.2 | 197.7 | 8.1 | 10 | 0.59 |
| | | 204.7 | 205.4 | 15.1 | 60.8 | 0.03 |
| | | 296.6 | 307.9 | 63.9 | 19.7 | 2.67 |
| | | 310.4 | 312.5 | 42.1 | 7.9 | 0.29 |
| | | 312.6 | 323.5 | 11.0 | 77.6 | 0.02 |
| 77 | 2.14 | 395.3 | 396.7 | 17.5 | 11.9 | 0.19 |
| | | 429.6 | 430.5 | 124.7 | 58.0 | 0.24 |
| | | 443.9 | 467.8 | 47.3 | 29.6 | 2.66 |
| | | 480.6 | 481.4 | 119.3 | 244.4 | 0.05 |
| | | 503 | 509.5 | 55.8 | 46.4 | 0.60 |
| | | 570 | 586.6 | 68.1 | 42.2 | 4.25 |
| | | 600 | 1452.5 | 3971.5 | 3903.2 | 3.43 |
| | | 159.4 | 173.7 | 140.6 | 52.4 | 11.20 |
| | | 174.7 | 194.9 | 14.6 | 11.7 | 0.42 |
| | | 201.6 | 204.5 | 29.2 | 73.7 | 0.13 |
| | | 297.9 | 307.9 | 25.6 | 17.6 | 1.72 |
| | | 314.1 | 317.0 | 182.8 | 231.9 | 0.17 |
| | | 391.6 | 393.5 | 10.0 | 10.9 | 0.34 |
| | | 429.6 | 430.5 | 367.5 | 333.4 | 0.29 |
| 200 | 2.16 | 448.0 | 456.8 | 29.4 | 43.8 | 4.07 |
| | | 456.9 | 478.4 | 428.7 | 328.4 | 0.07 |
| | | 480.5 | 481.4 | 374.7 | 315.1 | 0.01 |
| | | 564.9 | 579.9 | 38.1 | 49.9 | 4.52 |
| | | 598.0 | 1580.7 | 2900.5 | 3405.3 | 5.36 |
| | | | 315.7 | 100.3 | 402.1 | |
| | | 159.9 | 172.3 | 383.2 | 111.8 | 8.27 |
| | | 176.2 | 189.2 | 25.2 | 20.2 | 1.2 |
| | | 206.2 | 218.4 | 53.2 | 93.8 | 1.25 |
| | | 303 | 310.5 | 52.2 | 13.2 | 1.32 |
| | | 311.9 | 315.0 | 16.7 | 47.9 | 0.06 |
| | | 385.4 | 386.9 | 25.5 | 28.4 | 0.23 |
| 300 | 2.03 | 429.6 | 430.5 | 329 | 78 | 0.37 |
| | | 438 | 460.1 | 48.6 | 71.7 | 2.37 |
| | | 480.5 | 481.4 | 158.0 | 366 | 0.07 |
| | | 508.9 | 511.5 | 91.4 | 81.2 | 0.26 |
| | | 571 | 590.6 | 172.3 | 147.1 | 2.81 |
| | | 656.2 | 1765.9 | 2344.3 | 2922.8 | 8.35 |
| | | | 334.7 | 305.97 | 559.7 | |
| | | 161.0 | 175.2 | 361.6 | 79.2 | 9.15 |
| | | 176.2 | 193.3 | 19.5 | 18.0 | 0.33 |
| | | 201.2 | 203.4 | 30.9 | 86.1 | 0.11 |
| | | 297.9 | 307.9 | 43.7 | 38.8 | 1.35 |
| | | 394.3 | 396.7 | 158.5 | 171.2 | 0.39 |
| | | 429.6 | 430.5 | 358.1 | 72.5 | 0.26 |
| 350 | 2.03 | 443.9 | 466.9 | 59.6 | 48.2 | 2.66 |
| | | 480.5 | 481.4 | 86.6 | 430.8 | 0.05 |
| | | 509 | 511.5 | 123.6 | 75.4 | 0.25 |
| | | 571 | 590.6 | 157.1 | 133 | 2.82 |
| | | 653 | 1745.4 | 2791.3 | 3060.2 | 8.1 |
| | | | 368.2 | 188.9 | 144.1 | |
| | | 161.9 | 174.8 | 181 | 239.9 | 14.37 |
| | | 176.2 | 196.7 | 193.2 | 163.3 | 0.88 |
| | | 297.9 | 307.9 | 401 | 269.5 | 2.27 |
| | | 394.3 | 396.7 | 476.7 | 441.5 | 0.71 |
| | | 429.6 | 430.5 | 544.6 | 93.2 | 0.49 |
| 403 | 2.09 | 443.9 | 466.9 | 63.6 | 77.4 | 5.08 |
| | | 480.5 | 481.4 | 140.1 | 433.3 | 0.11 |
| | | 508.9 | 511.5 | 142.9 | 98.9 | 0.57 |
| | | 571 | 590.6 | 177.8 | 163.9 | 11.4 |
| | | 600 | 1989.7 | 3987.4 | 4208.4 | 5.41 |
| | | | 635.3 | 157.1 | 10.2 | |

TABLE II. Fitting parameters used in the dielectric function simulation for $PrNiO_3$.

| Temperature (K) | $\varepsilon_\infty$ | $\omega_{TO}$ ($cm^{-1}$) | $\omega_{LO}$ ($cm^{-1}$) $\omega_p$ ($cm^{-1}$) | $\gamma_{TO}$ ($cm^{-1}$) $\gamma_0$ ($cm^{-1}$) | $\gamma_{LO}$ ($cm^{-1}$) $\gamma_p$ ($cm^{-1}$) | $S$ ($cm^{-2}$) |
|---|---|---|---|---|---|---|
| | | 80.8 | 170.1 | 115.5 | 176.0 | 23.09 |
| | | 176.4 | 178.9 | 10.4 | 11.2 | 0.02 |
| | | 229.6 | 241.8 | 306.6 | 397.8 | 0.56 |
| | | 269.1 | 316.4 | 164.2 | 183.4 | 0.78 |
| 77 | 1.02 | 423.8 | 429.1 | 55.4 | 54.3 | 0.08 |
| | | 540.4 | 573.3 | 300.2 | 255.9 | 0.49 |
| | | 599.3 | 623.0 | 492.3 | 992.9 | 0.11 |
| | | 1362.2 | 2428.1 | 4580.8 | 5396.3 | 2.05 |
| | | | 447.57 | 84.91 | 1447.83 | |
| | | 88.5 | 160.5 | 20.3 | 958.7 | 37.08 |
| | | 187.6 | 189.6 | 18.5 | 17.7 | 0.18 |
| | | 229.6 | 241.8 | 865.2 | 171.3 | 1.69 |
| | | 269.1 | 316.4 | 113.4 | 181.9 | 2.32 |
| | | 423.8 | 429.1 | 70.4 | 86.8 | 0.31 |
| | | 540.4 | 573.3 | 624.9 | 416.4 | 3.54 |
| | | 599.4 | 1263.2 | 578.5 | 731.3 | 2.44 |
| 120 | 1.37 | 2155.3 | 2516.1 | 3000.1 | 3478.3 | 0.35 |
| | | | 1215.6 | 602.6 | 80.6 | |
| | | 88.3 | 161.5 | 26.8 | 873.7 | 32.75 |
| | | 192.3 | 195.9 | 39.7 | 56.3 | 0.29 |
| | | 232.6 | 243.9 | 749.3 | 96.3 | 1.24 |
| | | 277.9 | 328.3 | 64.7 | 77.4 | 2.28 |
| | | 423.8 | 429.1 | 38.4 | 38.3 | 0.25 |
| | | 540.4 | 573.3 | 1082.4 | 1335.7 | 3.02 |
| 140 | 1.03 | 599.7 | 1428.1 | 1434.7 | 1061.4 | 2.15 |
| | | 3311 | 3625.2 | 3051 | 4530 | 0.17 |
| | | | 1543.2 | 1549.9 | 98.6 | |
| | | 90.7 | 100.4 | 839.1 | 1866.8 | 5.12 |
| | | 177.9 | 179.7 | 159.4 | 59.6 | 0.74 |
| | | 229 | 339.0 | 596.0 | 163.5 | 11.85 |
| 300 | 1.01 | 542.0 | 1432.9 | 3069.6 | 1654.9 | 5.71 |
| | | 2933.7 | 3311.1 | 2618.2 | 5049.4 | 0.22 |
| | | | 1818.0 | 1795.0 | 904.9 | |

$$r(\omega)=\left(\frac{2}{\omega\tau\Delta}\right)\ln\{\omega\tau\Delta+[1+(\omega\tau\Delta)^2]^{1/2}\}-\left[\frac{2}{(\omega\tau\Delta)^2}\right]\{[1+(\omega t\Delta)^2]^{1/2}-1\}, \quad (5)$$

with

$$\Delta=2\varpi\tau \quad (6)$$

and

$$\tau^2=\frac{\left[\sinh\left(\frac{1}{2}\hbar\varpi\beta\right)\right]}{2\varpi^2\eta}. \quad (7)$$

$\sigma_1(\omega,\beta),\beta=1/kT$, is mainly three parameter dependent: $\sigma_{dc}=\sigma(0,\beta)$, the electrical conductivity (taken from our resistivity measurements); the frequency $\varpi_j$ that corresponds to the average between the transverse and the longitudinal optical mode of the $j$th reststrahlen band and $\eta$, characterizing the strength of the electron-phonon interaction, that is the average number of phonons that contribute to the polarization around a localized polaron. From them, the only actual parameter free to fit in each phonon contribution is $\eta$ because phonon frequencies are fixed by reflectivity and transmission measurements. The small polaron binding energy is given by $E_b \leqslant \varpi\eta/2$ (Refs. 6 and 10).

## REFLECTIVITY SPECTRA

The temperature-dependent reflectivity spectra of the $SmNiO_3$ and $PrNiO_3$ from 30 to 10 000 $cm^{-1}$ are shown in

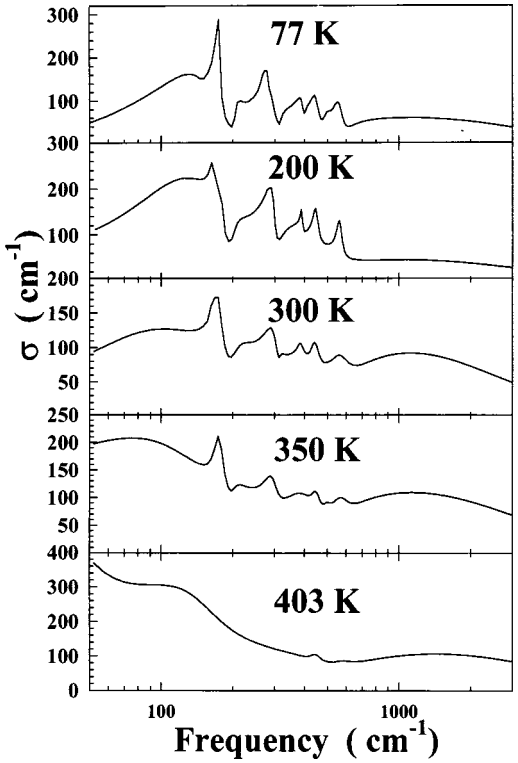


FIG. 4. Temperature dependence of the optical conductivity of $SmNiO_3$.

Figs. 2 and 3 respectively. In both cases the MI phase transition is detected as the spectrum evolves from low temperature typical insulator reflectivity, with well-defined phonon bands, to that expected for metal oxides at over $T_{MI}$ where reststrahlen bands are screened by delocalized mobile electrons. The overall results from reflectivity fits using the dielectric simulation are shown in Tables I and II. Keeping the physical meaning, the quoted numbers are to be understood as satisfying the convergence condition when the chi-squared test between the observed and expected data is less than $5.0\times10^{-5}$.

At 77 K, well-defined reflectivity features at $\sim$185 $cm^{-1}$ are assigned to lattice vibrations where the rare earth atom moves against the $NiO_6$ octahedral. The sharpness of these indicates a strong ionic environment, stronger in $SmNiO_3$, likely due to cations $R^{3+}$ ($R=$Sm, Pr) and $Ni^{3+}$ as already suggested for $NdNiO_3$ (Ref. 11). Phonon bands between 200 and 600 $cm^{-1}$ are associated with vibrations involving the motion of atoms belonging to $NiO_3$ octahedras. Between 200–400 $cm^{-1}$, they are related to deformation modes and bands between 400–600 $cm^{-1}$ are assigned to symmetric stretching modes symmetry allowed in the perovskite distorted $GdFeO_3$ lattice (*Pbnm*) of the insulating phase.[12] At low temperatures the phonon groups develop strong antiresonances close to longitudinal optical mode frequencies. We interpret this behavior in the reflectivity bands as indicating strong electron-phonon interactions for $RNiO_3$ ($R=$Pr, Sm). It probably reflects, as in $NdNiO_3$, high hybridization between Ni $3d$ and O $2p$ with the ionization $Ni^{2+}$ allowing self-trap electrons in the polarizable oxygen bonds. As noted in Ref. 11 although preparing our samples in a high-pressure oxygen atmosphere optimizes the $Ni^{3+}$ content these compounds really have bonds that are mixed state between $Ni^{3+}$ and $Ni^{2+}$. For both, $SmNiO_3$ and $PrNiO_3$, closer, but below $T_{MI}$, we were also able to deconvolute a weak Drude contribution (Tables I and II). Thus, knowing the plasma frequency, $\omega_p$, and using an estimate of the effective electron mass, $m^*\sim6$ to $11m_0$ ($m_0$, the free electron mass) (Ref. 13) we calculate [Eq. (3)] for each compound an effective number of carriers of the order of $N^*\sim10^{16}-10^{17}$ as expected for insulators.

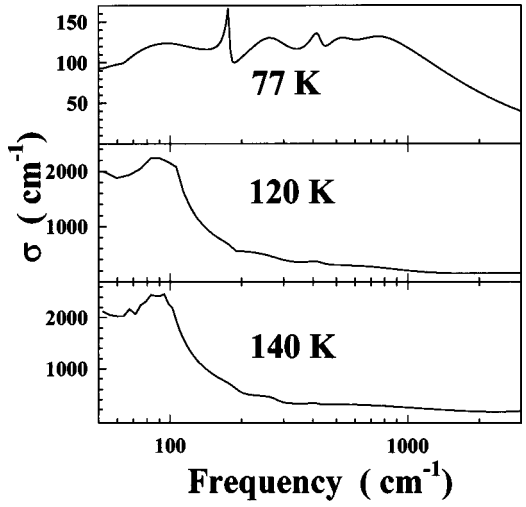


FIG. 5. Temperature dependence of the optical conductivity of $PrNiO_3$.

We also point to the vibrational mode absorptions of $SmNiO_3$ and $PrNiO_3$ (inset, Figs. 2 and 3, respectively). The comparison of the bands at 77 K shows that while those for $PrNiO_3$ are still partially screened the internal modes of $SmNiO_3$ have a splitting due to a progressive lower symmetry environment in the insulating phase. Thus, although we cannot conclude from this the existence of a superstructure, as it is discussed in Rodriguez-Carvajal *et al.*,[4] our spectra points to a significant low temperature distortion affecting the octahedra perhaps consequence of a more stable lattice for $SmNiO_3$ at 77 K or a partial manifestation of the Jahn-Teller character of $Ni^{3+}(t_{2g}^6e_g^1)$, more patent in $SmNiO_3$ than in precedent terms of the series due to the less pronounced covalent character of Ni-O interactions as $R$ size decreases. That splitting is not observed either in $NdNiO_3$ (Ref. 11) or $PrNiO_3$ (Fig. 3, inset) at the same temperature.

At temperatures higher than 135 K the reflectivity spectra of $PrNiO_3$ correspond to that of a metal oxide with a typical tail extending beyond 10 000 $cm^{-1}$ yielding at 140 K $\omega_p$ $\sim$1500 $cm^{-1}$ (Table II). Then, with $m^*\sim11m_0$ (Ref. 13) and Eq. (3) one is able to estimate the number of effective carriers as $N^*\sim10^{18}$, a value characteristic of a bad metal. In the transmission spectra of $PrNiO_3$ two very weak changes in the spectrum slope are found at 145 K, in the metallic phase (Fig. 3, inset), that were also reported for $NdNiO_3$ (Ref. 11) at about 470 and 1100 $cm^{-1}$. They are broadly related to one- and two-phonon density of states and to the fact that $PrNiO_3$ and $NdNiO_3$ are highly anharmonic (their crystallographic structure is near the orthorhombic-rombohedric limit). On the other hand, those features are not present in the transmission spectrum of the metallic phase of $SmNiO_3$, having a more stable orthorhombic lattice owed to heavier

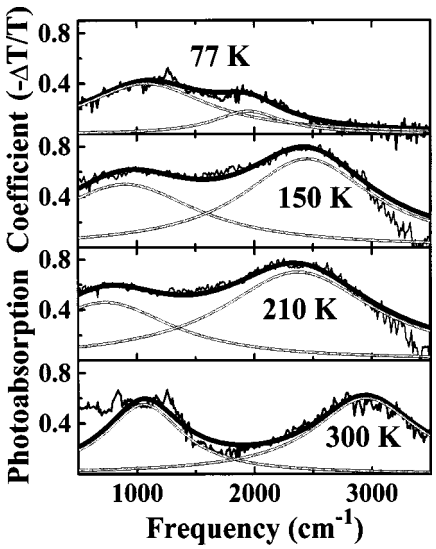


FIG. 6. Photoabsorption coefficient of $SmNiO_3$ at 77, 150, 210, and 300 K.

ions.[14] Here, we find at 460 K (inset, Fig. 2) partially screened traces of internal mode vibrational absorption bands.

The consequence of carrier increments due to the increase in temperature may also be seen in Figs. 4 and 5 where the infrared optical conductivity is shown at temperatures close to the MI phase transition of $SmNiO_3$ and $PrNiO_3$ respectively.

## PHOTOINDUCED ABSORPTION COEFFICIENT

In order to further understand the behavior of mobile electrons in the anharmonic lattice of $SmNiO_3$ and $PrNiO_3$, photoinduced transmission ($Tr_{photo}$) measurements were made at different temperatures and the corresponding photoabsorption coefficients $[-\Delta T/T=(Tr_{photo}-Tr/Tr)$ calculated.[15,16] Figures 6 and 7 show the temperature-dependent photoabsorption coefficient for $SmNiO_3$ and $PrNiO_3$ respectively. Lorentzians functions, $[A_j{*}C_j{}^2/(C_j{}^2+(\omega-\omega_j)^2)]$ (Tables III and IV), were used to distinguish the different bands that appear in the spectra. Weak and broad features are observed for $SmNiO_3$ centered at about

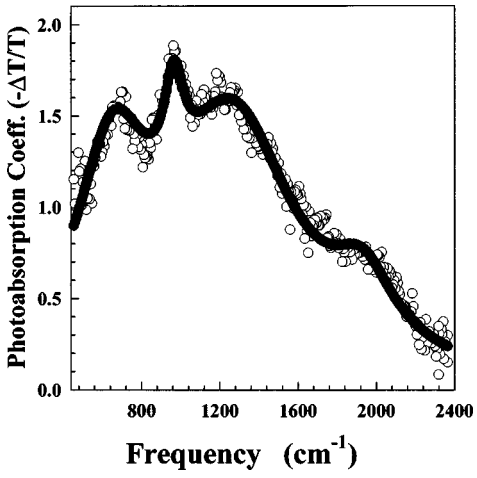


FIG. 7. Photoabsorption coefficient of $PrNiO_3$ at 77 K.

TABLE III. Lorentz parameters used in fitting the photoabsorption coefficient of $PrNiO_3$ at 77 K.

| $Aj$ | $Cj$ | $\omega j$ ($cm^{-1}$) |
|---|---|---|
| 1.10 | 227.1 | 651.8 |
| 0.54 | 62.6 | 965.9 |
| 1.40 | 385.8 | 1267.7 |
| 0.38 | 194.1 | 1932.0 |

1200 $cm^{-1}$ and 2000–3000 $cm^{-1}$ (Fig. 6) whereas for $PrNiO_3$ a set of weak bands appears in the range 400 to 5000 $cm^{-1}$ (Fig. 7). For this last compound, there is an absorption at ~650 $cm^{-1}$ that because its frequency position is probably due to a photoinduced infrared-activate phonon (i.e., a Raman mode infrared-active because of a photoinduced local distortion). This is followed by another feature at approximately 850 $cm^{-1}$ that is related to polaron bound states (see next section). At higher frequencies there are two broad bands and background that decrease in intensity asymptotically in the mid-infrared. We understand these last absorption bands as related higher order phonon contributions and to electronic transitions between polaronic sites where the energy associated to the photoabsorption peaks are approximately equal to the excited polaron binding energy $E_b$.[6,10] Photons in the mid-infrared range excite polaron hopping from a perturbed site to neighboring unperturbed sites, which is also accompanied by creation and annihilation of optical phonons. It also supports the introduction of non-Drude terms in the dielectric simulation of metallic $PrNiO_3$ (Table II).

We also note that in the photoabsorption coefficient of $SmNiO_3$ (Fig. 6) as temperature increases so does the definition and intensity of photoabsorption bands, specially the one associated to polarons with higher binding energy where this effect is more evident. This fact is in agreement with the idea of an increase of charge delocalization with temperature, because there are more thermally activated charges that are able hop from one polaronic site to another when they are photoexcited. In other words, temperature favors polaron mobility. In $PrNiO_3$, polarons have lower binding energies and hence are less localized than in $SmNiO_3$ at the same temperature; this is the reason why photoabsorption bands in the latter are weaker than in the first and intermediate relative to $NdNiO_3$ (Ref. 11).

## OPTICAL CONDUCTIVITY

As mentioned above, the optical conductivity of $SmNiO_3$ and $PrNiO_3$ in the 1500–5000 $cm^{-1}$ spectral region were

TABLE IV. Lorentz parameters used in fitting the photoabsorption coefficient of $SmNiO_3$ at different temperatures.

| Temperature (K) | $A_1$ | $C_1$ | $\omega_1$ ($cm^{-1}$) | $A_2$ | $C_2$ | $\omega_2$ ($cm^{-1}$) |
|---|---|---|---|---|---|---|
| 77 | 0.33 | 701 | 1061 | 0.22 | 401 | 1877 |
| 150 | 0.5 | 750 | 900 | 0.7 | 680 | 2450 |
| 210 | 0.46 | 700 | 730.6 | 0.7 | 790.7 | 2371 |
| 300 | 0.55 | 400 | 1060 | 0.6 | 550 | 2950 |

TABLE V. Parameters of the small polaron theory for $SmNiO_3$ and $PrNiO_3$. (Same cell two Gaussian contributions may be understood as essentially reflecting small differences in the vibrational environment.)

| | Temp (K) | $\sigma_{dc}$ ($cm^{-1}$) | $\eta_1$ | $\omega_1$ ($cm^{-1}$) | $\eta_2$ | $\omega_2$ ($cm^{-1}$) | $\eta_3$ | $\omega_3$ ($cm^{-1}$) |
|---|---|---|---|---|---|---|---|---|
| | 77 | 0.5 | 14 | 138 | 10 | 319 | 9.9 | 510.1 |
| | 200 | 4.0 | 14.5 | 161.5 | 6.7 | 563.4 | 7.1 | 1235 |
| $SmNiO_3$ | 300 | 28.11 | 10.43 | 164.7 | 4.97 | 592.87 | 4.79 | 1672.6 |
| | | | 5.6 | 140 | | | | |
| | 350 | 39.8 | 7.98 | 196.64 | 5.1 | 603.5 | 4.79 | 1887 |
| | 403 | 47.8 | 2.5 | 382.7 | 5.68 | 518.8 | 4.5 | 1756 |
| | 77 | 34.14 | 5.3 | 168 | 6.2 | 560 | 8.3 | 990 |
| $PrNiO_3$ | | | 5.4 | 295 | | | | |
| | 120 | 4780.1 | 1.04 | 300.5 | 4.34 | 1395.7 | | |

studied by means of the Reik and Heese[7] optical conductivity based on the small polaron approach. In this analysis we allow $\varpi$ (average phonon frequency) and $\eta$ (characterizing the strength of the electron-phonon interaction) to vary freely in the fit without losing their physical meaning. Electrical conductivity $\sigma_{dc}$, was calculated from the experimental resistivity (Fig. 1). Parameters used in the fittings are listed in Table V, whereas the experimental optical conductivity together with the corresponding estimates using Eq. (4) are shown in Figs. 8 and 9 for $SmNiO_3$ and $PrNiO_3$, respectively.

As we already found for $LaNi_{0.50}Fe_{0.50}O_3$ (Ref. 5), to reproduce an insulator conductivity in the infrared spectral range we only need to consider three independent terms of the type described by Eq. (4). The average frequencies, $\varpi_j$, are related to the vibrational modes of the simple perovskite lattice. In the insulating phase of the nickelates discussed here a good fit is achieved for both compounds considering between two and four independent polaronic contributions, which at 77 K are associated to lattice ($\approx$180 $cm^{-1}$), antisymmetric ($\approx$400 $cm^{-1}$), and symmetric ($\approx$500 $cm^{-1}$) stretching phonons. As temperature increases, lattice anharmonicity grows stronger and therefore a coupling between the different vibrational modes is expected. Because of this, the pointed phonons are replaced at higher temperatures, by an average phonon contribution ($\approx$350 $cm^{-1}$) together with overtones and phonon-sum processes (up to third order) that become more important especially when fitting the higher-frequency conductivity.

Based upon the conductivity parameters for $SmNiO_3$ listed in Table V, it is observed that at 77 K there are contributions from polarons with binding energies of 966 $cm^{-1}$ (0.12 eV; $\varpi_1 = 138\,cm^{-1}$) and 1595 $cm^{-1}$ (0.19 eV; $\varpi_2 = 319\,cm^{-1}$), respectively. The high $\eta$ values obtained for $SmNiO_3$ at 77 K, indicating very strong electron-phonon interactions, are in remarkable agreement with what it is expected from the pronounced temperature-dependent strong antiresonances, near longitudinal optical modes, seen in the reflectivity bands for each phonon group and related to the same fact. Photoinduced transmission spectrum at the same temperature exhibit well defined bands at about 1000 $cm^{-1}$ and 1800 $cm^{-1}$ (Table IV) which may be then associated to electronic excitations. In a similar way, polaronic contributions to the optical conductivity at 200 K with 1170 $cm^{-1}$ (0.14 eV; $\varpi = 161.5\,cm^{-1}$) and 1887 $cm^{-1}$ (0.23 eV; $\varpi = 563.4\,cm^{-1}$) binding energies coincide with photoabsorp-

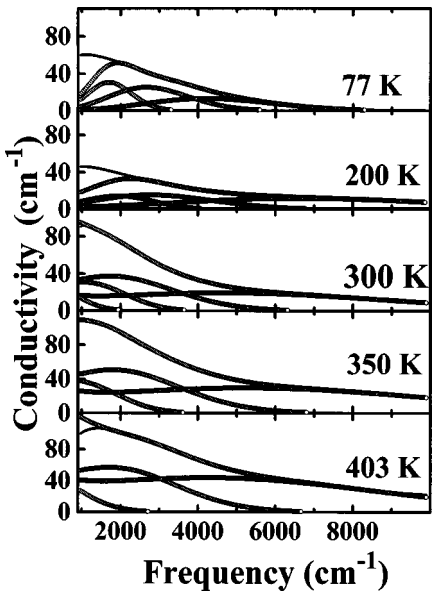


FIG. 8. Optical conductivity of $SmNiO_3$. Full lines, calculated from the respective reflectivity spectra; dotted lines, calculated using Eq. (3). The individual Gaussians correspond to the different phonon contributions.

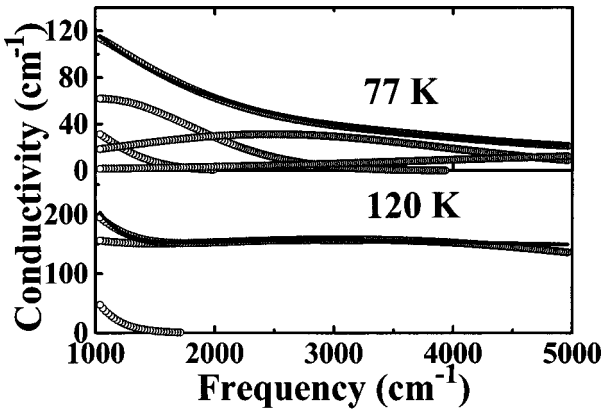


FIG. 9. Optical conductivity of $PrNiO_3$. Full lines, calculated from the respective reflectivity spectra; dotted lines, calculated using Eq. (3). The individual Gaussians correspond to the different phonon contributions.

tion bands at about 1100 $cm^{-1}$ and 2200 $cm^{-1}$, respectively.

Optical conductivity of $PrNiO_3$ at 77 K is the result of a four-polaronic contribution, which is also listed in Table V. Polarons with binding energies of 796 $cm^{-1}$ ($\varpi_1 = 295\ cm^{-1}$) and 1736 $cm^{-1}$ ($\varpi_2 = 560\ cm^{-1}$) are related to photoabsorption features centered at approximately 965 $cm^{-1}$ and 1267–1932 $cm^{-1}$, respectively. Interestingly, these last two values, although they correspond to a very weak band, peak in good agreement for a breathing frequency overtone and a phonon combination band and thus are also likely related to phonons assisting carrier hopping.

In $PrNiO_3$, charges are less localized than in $SmNiO_3$ at the same temperature, and therefore electron-phonon interaction should be weaker as it is revealed by the smaller values of $\eta$ obtained for the former. It is noted that the model in the finite-temperature approximation used here is not able to fit properly the optical conductivity calculated for $PrNiO_3$ at 140 K, after a steplike sharp decrease in the resistivity (Fig. 1), and at higher temperatures. We understand the failure of describing the experimental data as due to the poor reflectivity of as grown $PrNiO_3$ surfaces leading to smaller optical conductivities. It is known that the granular composition of ceramics, relative to single crystals, lowers the intrinsic specular reflection of a compound. In our spectra this results in a less prominent tail in the reflectivity spectra that, in turn, when fitted, translates into a lower plasma frequency. If we arbitrarily increase the measured reflectivities by a constant, the calculated parameters would be in better agreement with their expected physical interpretation. This is also reflected in that electrical conductivity ($\sigma_{dc}$) are about 6 (at 140 K) and 40 (at 300 K) times larger than the infrared extrapolated. Nevertheless it also points a change of carrier mobility that could be associated with the existence of larger polarons instead of small polarons regulating the localization regime.

The fit of optical conductivities achieved with the small polaron theory constitutes a valuable evidence of the relevant role played by phonons in the transport properties $SmNiO_3$ and $PrNiO_3$. This same behavior not only has been reported for $NdNiO_3$ (Ref. 11) but it has also been recently confirmed by an excellent agreement between experimental results obtained through $O^{16}$ with $O^{18}$ isotopic exchange and a simple model based in the existence of Jahn-Teller polarons in metallic-charge transfer systems.[17] Therefore, based upon quantitative evidence, we conclude that metal-insulator phase transitions in $RNiO_3$ ($R \neq La$) oxide compounds is definitely assisted by phonons through a mechanism involving delocalization of self-trapped electrons in a polaronic medium.

## CONCLUSION

Summarizing, we have measured temperature dependent reflectivity spectra of $RNiO_3$ ($R = Pr, Sm$) in the metallic and insulator phase and their photoabsorption coefficients. By analyzing the temperature behavior of phonon bands, the localization and the agreement between experimental and small polaron theoretically generated optical conductivities, we confirm the determinant participation of phonons in the transport properties of $RNiO_3$ ($R = Pr, Sm$). According to this, the metal-insulator transition in $SmNiO_3$ and $PrNiO_3$ is directly *related to self-trapped electrons in a polaronic medium at* $T_{MI}$.

## ACKNOWLEDGMENTS

M.A.M. is pleased to thank Professor R. Casali (Universidad Nacional del Nordeste) for his support and helpful discussions. This research has been partially supported by a grant (Grant No. 8017) of the National Research Council of Argentina (CONICET). Financial support by the Spanish CICYT (Comisión Interministerial de Ciencia y Tecnologia) under Project No. PB94-0096 is also acknowledged.

*Present address: Max Planck Institut für Strahlenchemie, Stiftstrasse 34-36, D-45470 Mülheim, Germany.
†Electronic address: nem@nahuel.biol.unlp.edu.ar

[1] For a recent review, see M. L. Medarde, J. Phys.: Condens. Matter **9**, 1 (1997), and references therein.
[2] G. Demazeau, A. Marbeuf, M. Pouchard, and P. Hagenmuller, J. Solid State Chem. **3**, 582 (1971).
[3] J. B. Torrance, P. Lacorre, A. I. Nazzal, E. J. Ansaldo, and Ch. Niedermayer, Phys. Rev. B **45**, 8209 (1992).
[4] J. Rodriguez-Carvajal, M. Medarde, P. Lacorre, M. T. Fernandez-Diaz, F. Fauth, and V. Trounov, Phys. Rev. B **57**, 456 (1998).
[5] J. A. Alonso, M. J. Martinez-Lope, and M. A. Hidalgo, J. Solid State Chem. **116**, 146 (1995).
[6] N. E. Massa, H. Falcón, H. Salva, and R. E. Carbonio, Phys. Rev. B **56**, 10 178 (1997), and references therein.
[7] H. G. Reik, in *Polarons in Ionic Crystals and Polar Semiconductors*, edited by J. Devreese (North-Holland, Amsterdam, 1972). Also, H. G. Reik and D. Heese, J. Phys. Chem. Solids **28**, 581 (1967).
[8] T. Holstein, Ann. Phys. (N.Y.) **8**, 343 (1959).
[9] R. Kubo, J. Phys. Soc. Jpn. **12**, 570 (1957).
[10] D. Emin, Phys. Rev. B **48**, 13 691 (1993).
[11] N. E. Massa, J. A. Alonso, M. J. Martinez-Lope, and I. Rasines, Phys. Rev. B **56**, 986 (1997).
[12] M. Couzi and P. Van Huong, J. Chim. Phys. Phys.-Chim. Biol. **69**, 1339 (1972).
[13] Estimates of the electron effective mass in nickelates vary from 6 to 11 free electron masses. See, for example, X. Granados, J. Fontcuberta, X. Obradors, Ll. Manosa, and J. B. Torrance, Phys. Rev. B **48**, 11 666 (1993); K. P. Rajeev *et al.*, Solid State Commun. **79**, 591 (1991).
[14] P. Lacorre, J. B. Torrance, J. Pannetier, A. I. Nazzal, P. W. Wang, and T. C. Huang, J. Solid State Chem. **91**, 225 (1991).
[15] G. B. Blanchet, C. R. Fincher, T. C. Hung, and A. J. Heeger, Phys. Rev. Lett. **50**, 1938 (1983).
[16] C. M. Foster, A. J. Heeger, G. Stucky, and N. Herron, Solid State Commun. **71**, 945 (1989).
[17] M. Medarde, P. Lacorre, K. Conder, F. Fauth, and A. Furrer, Phys. Rev. Lett. **80**, 2397 (1998).